Ionics (2020) 26:1057–1061
https://doi.org/10.1007/s11581-019-03315-8

BRIEF COMMUNICATION

A novel method for preparing α-$LiFeO_2$ nanorods for high-performance lithium-ion batteries

Youzuo Hu [1,2] · Xingquan Liu [1]

Received: 5 August 2019 / Revised: 2 October 2019 / Accepted: 20 October 2019 / Published online: 5 December 2019

Abstract

One-dimensional (1D) α-$LiFeO_2$ nanorods are successfully prepared via a low-temperature solid-state reaction from α-FeOOH nanorods synthesized by hydrothermal process and used as cathode materials in lithium-ion batteries. As cathode material for lithium-ion batteries, the nanorods can achieve a high initial specific capacity of 165.85 mAh/g at 0.1 C for which a high capacity retention of 81.65% can still be obtained after 50 cycles. The excellent performance and cycling stability are attributed to the unique 1D nanostructure, which facilitates the rapid electron exchange and fast lithium-ion diffusion between electrolyte and cathode materials.

Keywords α-$LiFeO_2$ nanorod · Energy storage and conversion · Nanocrystalline materials · Cathode

Introduction

Lithium-ion batteries (LIBs) have been widely used as renewable energy storage devices for electronic products and plug-in hybrid and pure electric vehicles due to their high-power density and stable cycling performance [1–3]. The layered α-$LiFeO_2$ is considered one of the potential candidates as cathode material for LIBs due to its high theoretical capacity (282 mAh/g), environmental friendliness, and low cost [4, 5]. However, there are still some challenges remained for α-$LiFeO_2$ cathodes, such as inherent sluggish kinetic and poor electronic conductivity, which severely disrupts the high-rate and cycling performance of batteries [6].

Generally, the nanostructured morphology such as nanowires, nanoparticles, and nanorods can enhance their material electrochemical properties [7–9]. Among different morphologies, one-dimensional (1D) nanorods have attracted numerous attentions due to their 1D transport pathway which enables good electron transport and fast lithium-ion insertion/removal [10]. However, there are still huge challenges to directly prepare α-$LiFeO_2$ nanorods via conventional strategies where cubic crystals are usually obtained [11]. According to previous reports, α-FeOOH nanorods have been used as a self-template to prepare 1D iron-based materials, such as Fe_2O_3 and Fe_3O_4 [12, 13]. Inspired by these, in this work, we firstly synthesize α-FeOOH nanorods by hydrothermal method; then, by solid-state reaction method, α-$LiFeO_2$ nanorods are obtained (Scheme S1). The excellent electrochemical performance of the as-prepared α-$LiFeO_2$ nanorods is evaluated in LIBs, and the structure-property relationship is explored based on physical characterization results.

Electronic supplementary material The online version of this article (https://doi.org/10.1007/s11581-019-03315-8) contains supplementary material, which is available to authorized users.

✉ Xingquan Liu
Lxquan@uestc.edu.cn

[1] R&D Center for New Energy Materials and Integrated Energy Devices, University of Electronic Science and Technology of China, Chengdu 610054, China

[2] Department of Chemistry, Lancaster University, Lancaster LA1 4YB, UK

Experimental

Material synthesis

α-FeOOH nanorods were synthesized through a hydrothermal process. Firstly, 2.59 g $Fe(NO)_3 \cdot 9H_2O$ and 1.01 g KOH were dissolved in 80 ml distilled water, and 1 ml of H_2O_2 was added to remove the Fe^{2+} in the solution. After thoroughly stirred for 1 h, the solution was transferred into a 100-ml Teflon-lined

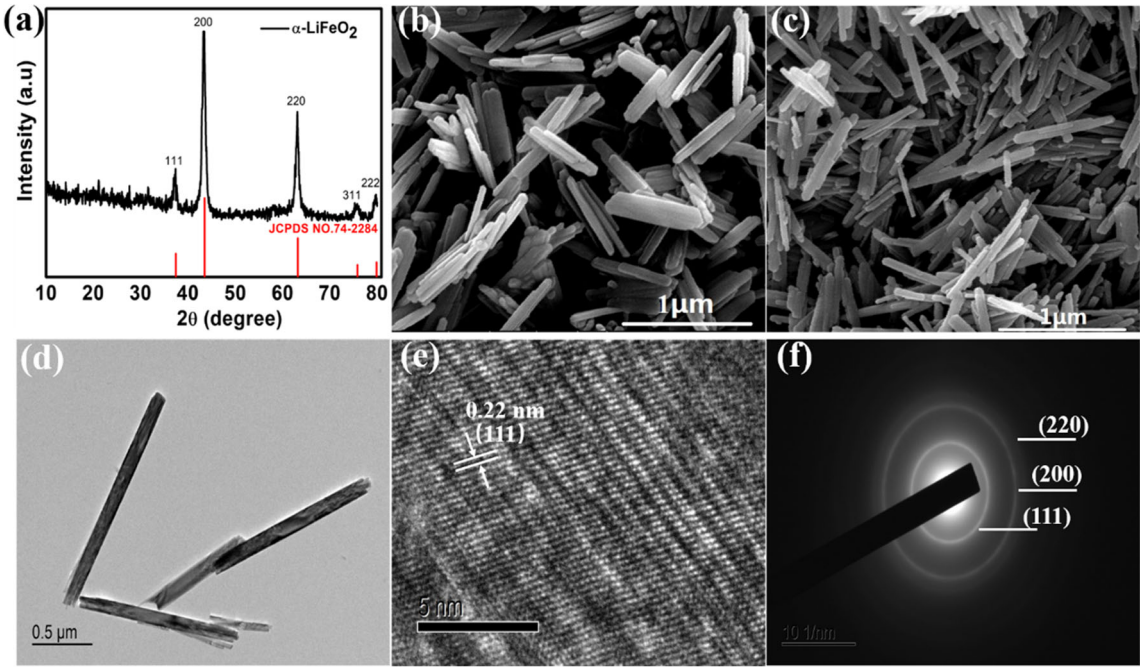

Fig. 1 **a** XRD pattern of the as-prepared α-$LiFeO_2$. **b** SEM image of α-FeOOH. **c** SEM, **d** TEM, and **e** HRTEM images with corresponding **f** SAED pattern of the as-prepared α-$LiFeO_2$

stainless steel autoclave and left at 100 °C for 6 h. α-$LiFeO_2$ nanorods were prepared via a low-temperature solid-state reaction method from the as-prepared α-FeOOH rods. Typically, the as-prepared α-FeOOH rods were mixed with $LiOH{\cdot}H_2O$ and $LiNO_3$ (Li^+/Fe^{3+} = 4) by grinding and then dried at room temperature. After that, the powder was sintered at 400 °C for 6 h in muffle to obtain α-$LiFeO_2$ nanorods.

Material characterization

XRD analysis, material morphologies, and electronic state of each element of the sample were characterized by X-ray diffraction (XRD, Bruker DX-1000, CuKα radiation), scanning electron microscopy (FESEM, JEOL, JSM-6360LV), transmission electron microscopy (TEM) and high-resolution transmission electron microscopy (HRTEM, JEOL, JEM-3010), and X-ray photoelectron spectroscope (XPS, ESCALAB 250XI), respectively.

Electrochemical measurements

For battery test, the working electrode was prepared from 85% as-prepared α-$LiFeO_2$ rods, 10% acetylene black, and 5% polyvinylidene fluoride. The lithium metal was used as counter electrode. The electrolyte was 1 M $LiPF_6$ in a mixture of ethylene carbonate, dimethyl carbonate, and ethylmethyl carbonate (EC:DMC:EMC, 1:1:1 by volume). The batteries were assembled in an argon-filled glove box and tested on Land cell Systems (LAND CT2001A) in the voltage range of 1.5–4.8 V. Cyclic voltammetry (CV) and electrochemical impedance spectroscopy (EIS) analysis were conducted with a CS-350 electrochemical workstation.

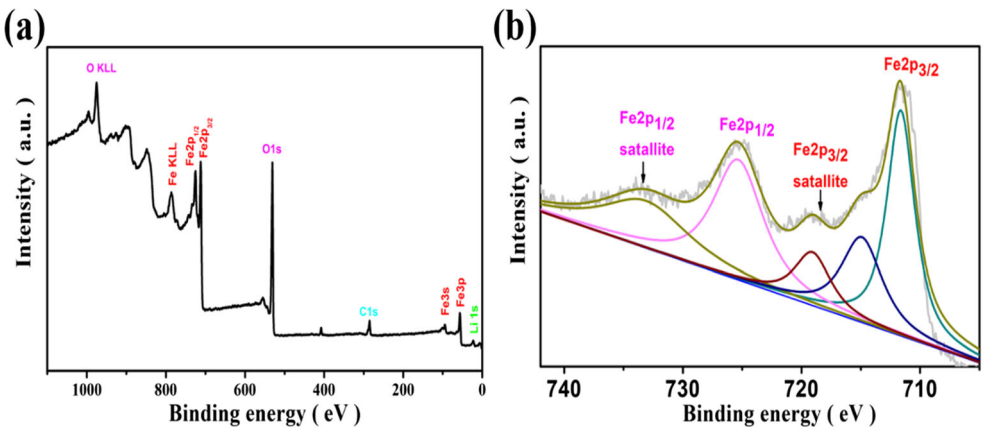

Fig. 2 **a** XPS survey and **b** Fe2p spectrum of α-$LiFeO_2$ nanorods

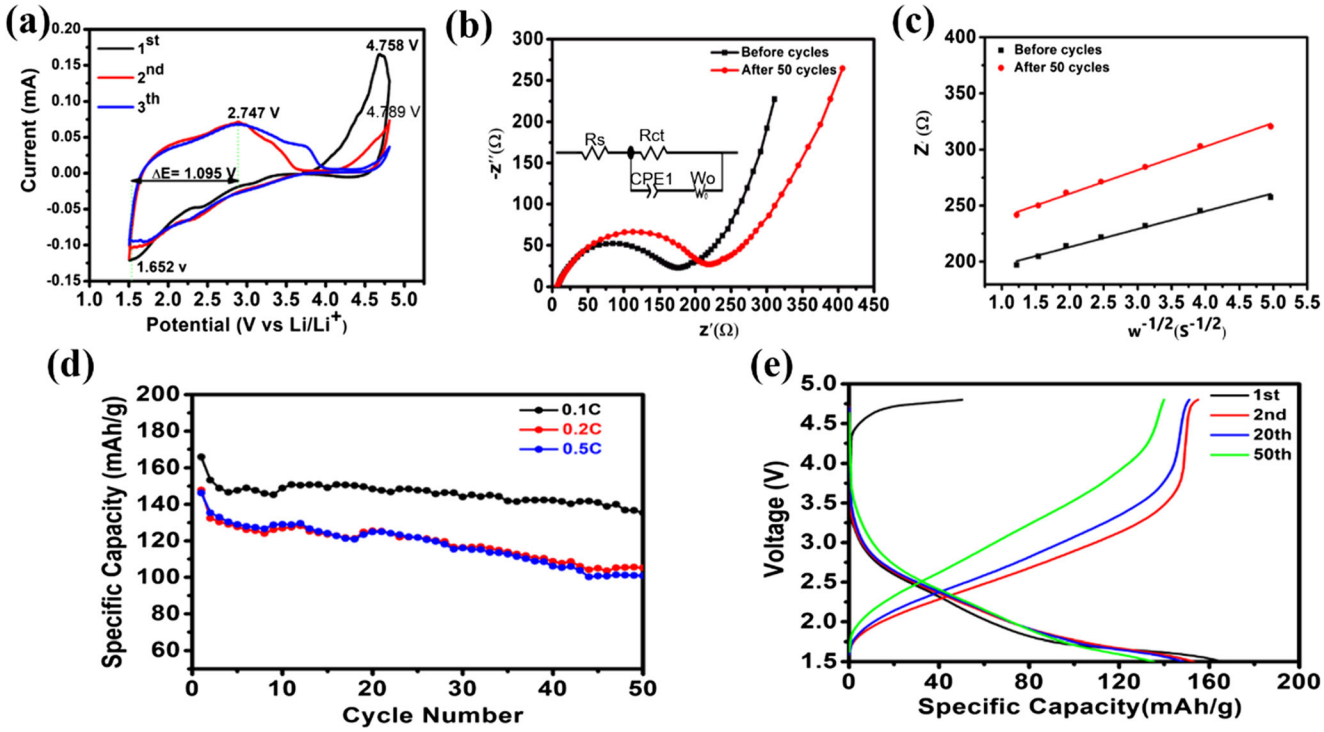

Fig. 3 **a** CV curves of the first three cycles, **b** Nyquist curves (the inset shows the equivalent circuit), **c** liner fitting curves of Z' vs $\omega^{-1/2}$, and **d** cycling performance of α-$LiFeO_2$ nanorods at 0.1, 0.2, and 0.5 C. **e** Specific charge-discharge curves at 0.1 C of α-$LiFeO_2$ nanorods

Results and discussion

XRD pattern of α-FeOOH nanorods is shown in Fig. S1. All peaks are indexed to α-FeOOH (Space group pbnm, JCPDS No. 29-0713) [14]. XRD pattern of α-$LiFeO_2$ nanorods (Fig. 1a) shows all the diffraction peaks (111), (200), (220), (311), and (222) are well regarded to the layered structure of α-$LiFeO_2$ (JCPDS No. 74-2284) with lattice constants a = 4.158 [14, 15]. No diffraction peak from α-FeOOH is observed, indicating the α-FeOOH nanorods are fully converted into α-$LiFeO_2$ in the low-temperature solid-state reaction.

The SEM image (Fig. 1b) shows the width and length of the α-FeOOH nanorods are approximately 20 nm and 0.75 μm, respectively. Figure 1c shows the morphology of the obtained α-$LiFeO_2$, which is mainly composed of nanorods, suggesting that the rod-like morphology of the α-FeOOH nanorods is remained after the solid-state reaction.

TEM image (Fig. 1d) further confirms the diameter of α-$LiFeO_2$ nanorods is around 20 nm. The HRTEM image in Fig. 1e shows the lattice fringe spacing of 0.24 nm is consistent with the (111) crystal planes of α-$LiFeO_2$. The corresponding selected area electron diffraction (SAED) pattern presented in Fig. 1e shows the diffraction rings from inside to outside as (111), (200), and (220), which are in good agreement with the XRD results.

The XPS survey of the α-$LiFeO_2$ nanorods (Fig. 2a) confirms that the sample comprises Li, Fe, and O. The spectrum of Fe2p is depicted in Fig. 2b. The Fe2p spectrum exhibits two peaks at 711.15 eV and 724.89 eV, corresponding to Fe 2p3/2 and Fe 2p1/2 spin orbit peaks of α-$LiFeO_2$, respectively. Besides, both Fe 2p3/2 and Fe 2p1/2 main peaks show satellite peaks on their higher binding energy sides, thus confirming the Fe (III) oxidation state [16].

CV, EIS, and charge-discharge curves of the α-$LiFeO_2$ nanorods are depicted in Fig. 3 together with its cycling performance. Figure 3a shows CV curves in the voltage range of 1.5–4.8 V. The oxidation peaks appeared at 2.74 and 4.75 V are attributed to the charge process, and cathodic peaks at 1.65 V are associated with lithium insertion in the α-$LiFeO_2$ nanorods [17]. Figure 3b displays Nyquist plots of the α-$LiFeO_2$ electrode before and after 50 cycles of cycling at 0.1 C. Both figures contain a semicircle and a diagonal line representing the charge transfer resistance (R_{ct}) and the Warburg impedance (ω_o), respectively [18, 19].

Table 1 lists the fitting value of charge transfer resistance (R_{ct}) of α-$LiFeO_2$ nanorods in batteries. The charge transfer resistance is 151.5 and 183 Ω before and after 50 cycles, respectively. The small potential difference (ΔE = 1.095 V) and impedance change value (ΔR_{ct} = 31.5 Ω) indicate that the

Table 1 Fitting values of charge transfer resistance (R_{ct}) and lithium-ion diffusion coefficient of the α-$LiFeO_2$ electrode

	0 cycle	50 cycles
Charge transfer resistance/Ω (R_{ct})	151.5	183
D_{Li}^+/cm^2 s^{-1}	2.7×10^{-12}	1.5×10^{-12}

rod-like α-$LiFeO_2$ has a good electronic conductivity [20–22]. The lithium-ion diffusion coefficient can be calculated using following equations [23]

$$D_{Li^+} = \frac{R^2T^2}{2A^2n^4F^4C^2\sigma^2} \quad (1)$$

where D_{Li}^+ is the lithium-ion diffusion coefficient, A is surface area of the electrode, R is gas constant, n is number of electrons, T is absolute temperature, F is the Faraday constant, C is the Li-ion concentration in the electrode, and σ is the Warburg factor shown in Fig. 3c. The D_{Li}^+ value of the α-$LiFeO_2$ electrode is also listed in Table 1. The decrease of D_{Li}^+ value after the 50 cycles is small, suggesting that one-dimensional ion transport channel provided by the nanorod structure improves the Li-ion diffusion rate and enables a better rate capability of α-$LiFeO_2$.

Figure 3 d and e show the cycling performance of α-$LiFeO_2$ nanorod electrodes at 0.1, 0.2, and 0.5 C. The cycling performance of α-$LiFeO_2$ is tested at 0.1, 0.2, and 0.5 C within the voltage range of 1.5–4.8 V (Fig. 3d). The initial discharge capacities of α-$LiFeO_2$ are 165.85, 150.84, and 147.87 mAh/g, and these drop to 135.42, 105.23, and 100.88 mAh/g after 50 cycles, respectively. Compared with α-$LiFeO_2$ bulk samples reported in literature [17, 24], the α-$LiFeO_2$ nanorod electrode here delivers a better cycling performance at 0.2 and 0.5 C, which can be ascribed to the nanorod morphology which is beneficial for electron and lithium-ion transportation [24, 25]. The charge/discharge profiles (Fig. 3e) remain nearly the same after 50 cycles, suggesting a very small polarization during cycling process.

Conclusion

We successfully prepared α-$LiFeO_2$ nanorods via a novel hydrothermal-assisted solid-state method by using α-FeOOH nanorods as the self-sacrifice template. The α-$LiFeO_2$ nanorod can provide one-dimensional path facilitating the transportation of lithium-ions. Moreover, the good electron transport property of one-dimensional nanorods reduces the charge transfer impedance and thus also improves the electrode cycling performance. As a result, the α-$LiFeO_2$ nanorod electrode presents a stable specific capacity of 139.8 mAh/g^{-1} at 0.1 C after 50 cycles, indicating the enhancement effect of the nanorod morphology for electrochemical applications.

Funding information This work was financially supported by the National Natural Science Foundation of China (No. 21071026) and the Outstanding Talent Introduction Project of University of Electronic Science and Technology of China (No. 08JC00303).

References

1. Zubi G, Dufo-López R, Carvalho M, Pasaoglu G (2018). The lithium-ion battery: State of the art and future perspectives. Renew Sust Energ Rev 89:292–308
2. Armand M, Tarascon JM (2008) Building better batteries. Nature 451:652–657
3. Nitta NK, Fei X, Wu J, Lee T, Yushin G (2015) Li-ion battery materials: present and future. Mater Today 18:252–264
4. Li JG, Li JJ, Luo J, Wang L, He XM (2011). Recent Advances in the $LiFeO_2$ -based Materials for Li-ion Batteries. Int J Electrochem Sci 6:1550–1561
5. Sakurai Y, Arai H, Okada S, Yamaki J (1997). Low temperature synthesis and electrochemical characteristics of $LiFeO_2$ cathodes. J Power Sources 68:711–715
6. Kanno R, Shirane T, Kawamoto Y, Takeda Y, Takana M, Ohashi M, Yamaguchi Y, Electrochem J (1996). Synthesis, Structure, and Electrochemical Properties of a New Lithium Iron Oxide, $LiFeO_2$, with a Corrugated Layer Structure. Soc 143:2435–2442
7. Li CL, Bai NB, Chen H, Lu HY, Xiang KX (2015) Preparation and characterization $LiFePO_4$/C nanowires and their improved performance for lithium-ion batteries. Ionics 21:2465–2469
8. Pignanelli F, Romero M, Mombrú D, Téliz E, Díaz V, Castiglioni J, Zinola F, Faccio R, Mombrú ÁW (2019). Insights of cobalt doping on carbon-coated $LiFePO_4$ olivine nanoparticles prepared by citric acid combustion route as cathodes for lithium batteries. Ionics 25: 3593–3601
9. Xue L, Zhang QH, Zhu XH, Gu L, Yue JL, Xia QY, Xing T, Chen TT, Yao Y, Xia H (2019) 3D $LiCoO_2$ nanosheets assembled nanorod arrays via confined dissolution recrystallization for advanced aqueous lithium-ion batteries. Nano Energy 56:463–472
10. Cheng Y, Feng K, Song ZH, Zhang HZ, Li XF, Zhang HM (2018) Li_{0.93}V_{2.07}BO₅: a new nano-rod cathode material for lithium ion batteries. Nanoscale 10: 1997–2003
11. Kanno R, Shirane T, Inaba Y, Kawamoto Y (1997). Synthesis and electrochemical properties of lithium iron oxides with layer-related structures. J Power Sources 68:145–152
12. Chen MH, Liu JL, Chao DL, Wang J, Yin JH, Lin JY, Fan HJ, Shen ZX (2014). Porous α-Fe_2 O_3 nanorods supported on carbon nanotubes-graphene foam as superior anode for lithium ion batteries. Nano Energy 9:364–372
13. Ma YT, Huang J, Lin L, Xie QS, Yan MY, Qu BH, Wang LS, Mai LQ, Peng DL (2017). Self-assembly synthesis of 3D graphene-encapsulated hierarchical Fe_3 O_4 nano-flower architecture with high lithium storage capacity and excellent ratecapability. J Power Sources 365:98–108
14. Rahman MM, Glushenkov AM, Chen ZQ, Dai XJ (2013) Phys Chem Chem Phys 15:20371–20378
15. Hu CF, Shang YY, Wang Y, Xu J, Zhang YJ, Li XJ, Cao AY (2017). A flexible gas sensor based on single-walled carbon nanotube-Fe_2 O_3 composite film. Appl Surf Sci 405:405–411
16. Shilpa A, Sharma J (2017). Template-free synthesis of hollow Li_2 O–Fe_2 O_3 –Ag heterostructures for ultra-high performance Li-ion batteries. Mater Chem A 5:14220–14229
17. Abdel-Ghany AE, Mauger A, Groult H, Zaghib K, Julien CM (2012). Structural properties and electrochemistry of α-$LiFeO_2$. J Power Sources 197:285–291
18. Moralesa J, Santos-Pe J, Trocolia R, Frangerb S (2008). Insights into the electrochemical activity of nanosized α-$LiFeO_2$. Electrochim Acta 53:6366–6371

19. Chen ZY, Yan XY, Xu M, Cao KF, Zhu HL, Li LJ, Duan JF (2017). Building Honeycomb-Like Hollow Microsphere Architecture in a Bubble Template Reaction for High-Performance Lithium-Rich Layered OxideCathode Materials. Mater Interfaces 9:30617–30625
20. Longonia G, Pandaa JK, Gagliania L, Bresciab R, Mannac L, Bonaccorsoa F, Pellegrinia V (2018). In situ $LiFePO_4$ nanoparticles grown on few-layer graphene flakes as high-power cathode nanohybrids for lithium-ion batteries. Nano Energy 51:656–667
21. Wu B, Gao WL (2018). $LiMn_{0.7}$ $Fe_{0.3}$ PO_4 nanorods grown on graphene sheets synthesized in situ by modified microwave-assisted solvothermal method as highperformancecathode materials. J Mater Sci 53:4433–4443
22. Xu M, Chen ZY, Zhu HL, Yan XY, Li LJ, Zhao QF (2015). Mitigating capacity fade by constructing highly ordered mesoporous Al_2 O 3/polyacene double-shelled architecture in Li-rich cathode materials. J Mater Chem A 3:13933–13945
23. Zhao HY, Liu SS, Liu XQ, Tan M, Wang ZW, Cai Y, Komarneni S (2016). Orthorhombic $LiMnO_2$ nanorods as cathode materials for lithium-ion batteries: Synthesis and electrochemical properties. Ceram Int 42:9319–9322
24. Morales J, Santos-Pena J (2007). Highly electroactive nanosized α-$LiFeO_2$. Electrochem Communications 9:2116–2120
25. Xu M, Chen ZY, Li LJ, Zhu HL, Zhao QF, Xu L, Peng NF, Gong L (2015). Highly crystalline alumina surface coating from hydrolysis of aluminum isopropoxide on lithium-rich layered oxide. J Power Sources 281:444–454